Effect of Temperature on the Solid-state Molecular Structure of $[Fe_3(CO)_{12}]$†

Dario Braga,*[a] Fabrizia Grepioni,[a] Louis J. Farrugia[b] and Brian F. G. Johnson[c]

[a] *Dipartimento di Chimica 'G. Ciamician', Università di Bologna, Via Selmi 2, 40126 Bologna, Italy*

[b] *Department of Chemistry, The University of Glasgow, Glasgow G12 8QQ, UK*

[c] *Department of Chemistry, The University of Edinburgh, West Mains Road, Edinburgh EH9 3JJ, UK*

The molecular and crystal structure of $[Fe_3(CO)_{12}]$ has been reinvestigated from single-crystal X-ray diffraction data collected at 100, 160, 250 and 320 K. The asymmetric bridging carbonyl ligands become progressively more symmetric as the temperature is decreased. At the lowest temperature the molecule possesses nearly exact C_{2v} symmetry. The crystal structure has been examined in the two limiting hypothetical $P2_1$ and $P1$ crystals composing the disordered $P2_1/n$ structure.

Dodecacarbonyltriiron, $[Fe_3(CO)_{12}]$, occupies a special place in metal carbonyl cluster chemistry and a number of papers concerning either the static or the dynamic structure of $[Fe_3(CO)_{12}]$ in both solution and in the solid state have been written.[1-11] Such an interest in structural chemistry is usually associated with disagreement in the interpretation of experimental evidence or with the mismatch between theoretical prediction and experimental findings as, for example, in the case of ferrocene.[12,13] Both $[Co_2(CO)_8]$ and $[Fe_2(CO)_9]$ and their interrelationship have also been subjected to debate.[14] To date, not one of these structural problems has been completely resolved. However, a deeper knowledge of these complex structural systems has been achieved, in recent years, by enlarging the perspective from that focussed on the structure of the *isolated* molecule to that of the structure of the molecule in its crystalline environment.[15]

There are excellent accounts available where the 'saga' of $[Fe_3(CO)_{12}]$ is recounted.[16] The reader is addressed to these papers. We only wish to summarize briefly here some key aspects of the spectroscopic and theoretical studies.

The cluster $[Fe_3(CO)_{12}]$ undergoes isomerization in solution. At room temperature the IR spectrum consists of two strong bands in the terminal ν_{CO} stretching region and two weak bands in the ν_{CO} bridging region. Only at 20 K in an argon matrix is the IR spectrum consistent with the presence of two bridging and ten terminal CO ligands.[1a]

The solution ^{13}C NMR spectrum of $[Fe_3(CO)_{12}]$ remains a sharp singlet down to -150 °C. Several different mechanisms have been put forward to account for this extreme structural flexibility and a number of studies have been conducted on derivatives of $[Fe_3(CO)_{12}]$ in order to gain indirect insight into the fluxional process.[2]

This solution behaviour has prompted the elaboration of alternative models to explain the rearrangements that $[Fe_3(CO)_{12}]$ and other binary carbonyls undergo in solution. To account for this dynamic phenomenon the idea that the metal-atom skeleton undergoes librational motion within the quasi-octahedral shell of ligands was suggested together with the interconversion of the icosahedral ligand shell through an anticubeoctahedral complementary geometry. More recently,[3d] is has been argued that a concerted bridge opening-closing mechanism could also explain the experimental observations.

Carbon-13 cross-polarization magic angle spinning NMR experiments have shown[4] that the solid-state spectrum of $[Fe_3(CO)_{12}]$ is markedly temperature dependent. At 297 K the spectrum consists of three signals of similar integrated intensity, whereas at 178 K the spectrum is said to be consistent with the 'observed solid-state' structure. This assignment has been recently questioned, and the alternative suggestion that an averaging mechanism is still operating at that temperature has been put foward.[4d] The original proposition for the interpretation of these spectral features, however, was based on rotational jumps of the iron triangle within the carbonyl ligand shell. The same model has been adopted by others.

The Mössbauer spectrum of $[Fe_3(CO)_{12}]$ has been determined on several occasions. In the most recent of these studies[5b] it has been shown that the spectra reveal an unusual temperature dependance, which has been related to changes in orbital populations resulting from changes in the iron–iron and/or iron–carbon bond length. {The same authors anticipated that the collection of a low temperature data set on $[Fe_3(CO)_{12}]$ could have afforded insight into the interpretation of this phenomenon.}

Analysis of the iron K-edge extended X-ray absorption fine structure (EXAFS) data with multiple scattering showed that $[Fe_3(CO)_{12}]$ in light petroleum solution is present mainly as the all terminal structure whereas in the more polar medium of a frozen CH_2Cl_2 solution the bridged structure is favoured.[6]

The room-temperature molecular structure of $[Fe_3(CO)_{12}]$ was first established by Wei and Dahl[7a] by single-crystal X-ray diffraction. The authors also discussed the nature of the crystallographic disorder observed in the crystal. Cotton and Troup[7b] were subsequently able to resolve the light-atom positions, and obtained an image of the molecular structure characterized by the well known C_2 symmetric distribution of CO ligands with two asymmetric bridging carbonyls spanning the shortest iron–iron edge [2.558(1) *vs.* 2.677(2) and 2.683(1) Å at 295 K] and ten terminal ligands. The idealized two-fold axis passes through the middle of the bridged iron–iron bond and the opposite iron atom. Disorder in crystalline $[Fe_3(CO)_{12}]$ arises because the molecule is located around an inversion centre which results from the space average of molecules in two centrosymmetric orientations. It has been argued that the oxygen atoms describe a distorted icosahedron, and because an icosahedron is invariant to inversion, the $[Fe_3(CO)_{12}]$ crystal can be seen as being composed of $[Fe_3(CO)_{12}]$ molecules randomly distributed throughout the lattice in two centrosymmetric orientations. An alternative interpretation of the disorder is based on the possible occurrence of 60°

† *Supplementary data available:* see Instructions for Authors, *J. Chem. Soc., Dalton Trans.*, 1994, Issue 1, pp. xxiii–xxviii.

Non-SI unit employed: cal = 4.184 J.

reorientational jumps of the iron triangle within the CO ligand shell. In this dynamic model of disorder the 'star-of-David' generation is due to the time average inherent in the diffraction experiment. The reorientational jump model has been invoked to account for some solid-state NMR spectral features, as discussed above.[4b,c] In a third hypothesis, the $[Fe_3(CO)_{12}]$ crystal is seen as constituting an overall 'composite disordered macro structure' formed by twinning of ordered cells with axes multiple of the average one. This situation has been observed in the crystal of the related molecule $[Fe_2Os(CO)_{12}]$.[8] The molecular self-recognition and crystal-building process in solid $[Fe_3(CO)_{12}]$ and $[Ru_3(CO)_{12}]$ have also been recently investigated by empirical atom–atom pairwise packing potential-energy calculations.[9]

It has been demonstrated,[10] on the basis of the Cotton and Troup [7b] data, that the orientation of the iron atom anisotropic displacement parameters at room temperature is indicative of a preferential librational motion of the iron triangle about the idealized two-fold axis rather than an in-plane motion of the type required by the reorientation of the iron triangle *via* 60° jumps in the solid state.

The structure of $[Fe_3(CO)_{12}]$ has been investigated by various empirical and semi-empirical methods. In molecular mechanics simulations [11a] the calculated C_{2v} structure agrees to a reasonable extent with the experimental one, although the latter presents a more extensive asymmetry of the bridging ligands (see below). Recent SINDO1 calculations [11b] have been used to study the carbonyl fluxionality and the electronic structure of $[Fe_3(CO)_{12}]$. It has been shown that the bridge closing-opening mechanism is the lowest energy process and that the difference in structure between $[Fe_3(CO)_{12}]$, $[Ru_3(CO)_{12}]$ and $[Os_3(CO)_{12}]$ has an electronic origin. The importance of steric factors in determining the ligand distributions in these complexes has also been addressed.[11c]

In view of this widespread and continuing interest in $[Fe_3(CO)_{12}]$ and of the controversial interpretation of the dynamic behaviour of this species in solution and in the solid state, we have undertaken a systematic investigation of the molecular and crystal structure of $[Fe_3(CO)_{12}]$ as a function of temperature. To this purpose we have collected various X-ray diffraction data sets on $[Fe_3(CO)_{12}]$ crystals between 100 and 320 K and investigated the structure of the crystal by means of empirical packing potential-energy calculations and packing analysis. These methods have been successfully applied to several organometallic solid-state problems concerning both crystalline mononuclear and polynuclear cluster complexes.[15] Part of this work has been the subject of a preliminary communication.[7c]

In this paper the experimental molecular structure of $[Fe_3(CO)_{12}]$ and the temperature variation of its structural characteristics is discussed. The atomic anisotropic displacement parameters for the iron atoms and the possible librational models are then analysed to describe the dynamic part of the disorder observed in the experimental crystal structure at the various temperatures. Finally, we discuss the behaviour with temperature of the crystal structure in terms of the packing coefficient, the empirical packing potential energy and the intermolecular contacts.

Results and Discussion

Molecular Structure of $[Fe_3(CO)_{12}]$ *at Different Temperatures.*—Single-crystal X-ray diffraction data for $[Fe_3(CO)_{12}]$ have been collected at 320, 250, 160 and 100 K (see Experimental section).[7c] The change with temperature of the unit-cell axes and volume is reported in Table 1. As the temperature decreases the crystal retains the monoclinic structure. The 'average' structure is described by the centrosymmetric space group $P2_1/n$ with two molecules located around a crystallographic centre of inversion. This operator generates the well known 'star-of-David' with the two metal triangles in opposite orientations. As described earlier,[7a,b] the near-centrosymmetry of the icosahedral ligand distribution causes overlap of the carbonyl ligands with atoms belonging to the two images at a distance close to experimental resolution. In our experiments there is no trace, down to 100 K, of phase transitions to other crystal systems or to the non-centrosymmetric space group $P2_1$, hence the relative population of the two images is 50% and the disorder is retained.

Structural parameters relevant to the following discussion are compared in Table 2. An ORTEP [17] drawing of the structure at 100 K is shown in Fig. 1 together with the labelling scheme. As can be seen from Table 2, the temperature greatly affects the molecular structure of $[Fe_3(CO)_{12}]$. The bridging ligands become progressively more symmetric, this being accompanied by a congruent decrease in the bridged Fe–Fe bond length [from 2.554(1) at 320 to 2.540(1) Å at 100 K]. A simplified representation of the $Fe(\mu\text{-}CO)_2Fe$ system at the two extreme

Table 1 Unit-cell parameters and volumes for crystalline $[Fe_3(CO)_{12}]$ at different temperatures

T/K	a/Å	b/Å	c/Å	β/°	U_{cell}/Å^3
320	8.375(2)	11.330(2)	8.882(4)	97.00(3)	836.5(4)
295 [7b]	8.359(2)	11.309(2)	8.862(2)	97.00(1)	831.5
250	8.304(2)	11.231(4)	8.822(3)	96.89(4)	816.8(4)
160	8.221(4)	11.128(3)	8.760(4)	96.99(3)	795.4(6)
100	8.174(2)	11.090(2)	8.722(3)	96.90(2)	784.9(4)

Table 2 Relevant structure parameters for $[Fe_3(CO)_{12}]$ at various temperatures

	T/K			
	320	250	160	100
Fe(1)–Fe(3)	2.679(1)	2.682(2)	2.684(2)	2.682(1)
Fe(1)–Fe(2)	2.674(1)	2.677(2)	2.674(2)	2.675(1)
Fe(2)–Fe(3)	2.554(2)	2.551(2)	2.545(2)	2.540(1)
Fe(2)–C(1)	2.25(3)	2.10(2)	2.02(3)	2.00(1)
Fe(3)–C(1)	2.04(3)	1.97(2)	1.96(3)	1.95(1)
C(1)–O(1)	1.13(2)	1.10(3)	1.16(2)	1.156(13)
Fe(2)–C(2)	1.95(2)	1.99(1)	2.02(3)	2.00(1)
Fe(3)–C(2)	2.24(2)	2.11(1)	2.08(3)	2.05(1)
C(2)–O(2)	1.11(2)	1.14(2)	1.13(4)	1.140(12)
Fe–C(terminal)	1.82	1.82	1.82	1.82
C–O(terminal)	1.11	1.14	1.15	1.15
Fe(2)–C(1)–Fe(3)	74.1(5)	77.5(8)	79.4(7)	80.0(5)
Fe(2)–C(2)–Fe(3)	74.7(7)	77.0(3)	76.9(13)	77.5(5)

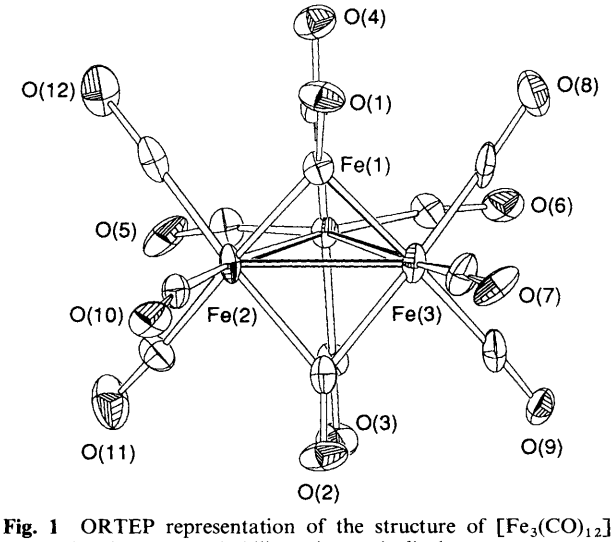

Fig. 1 ORTEP representation of the structure of $[Fe_3(CO)_{12}]$ at 100 K showing 50% probability anisotropic displacement parameters

temperatures (320 and 100 K) is shown in Fig. 2. The other two Fe–Fe bonds do not change appreciably with respect to the room temperature structure [2.679(1)–2.682(1) and 2.674(1)–2.675(1) Å]. The Fe–Fe bond lengths determined by Cotton and Troup [7b] fit almost perfectly in this trend [2.683(1), 2.677(2) and 2.558(1) Å]. One may object to the significance of these structural changes because of the relatively high bond length estimated standard deviations. While this is true for the individual values, we believe that the overall trends shown by both the degree of asymmetry of the bridging ligands and the length of the more accurately defined Fe–Fe bonds are trustworthy.

The structural parameters obtained at the lowest temperature (100 K) can be compared with the data available for

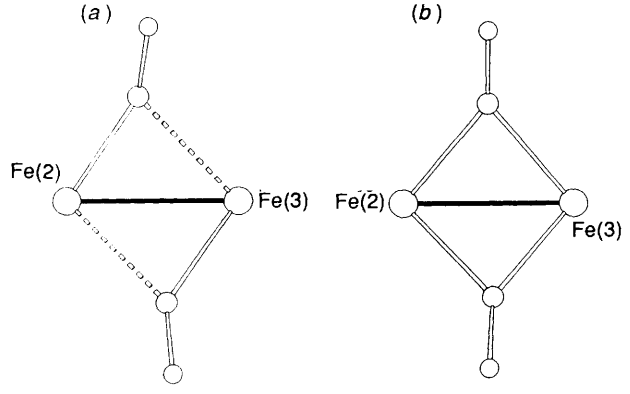

Fig. 2 A simplified representation of the $(OC)_3Fe(\mu\text{-}CO)_2Fe(CO)_3$ system at the two extreme temperatures. Note how the markedly asymmetric bridging carbonyl ligands at 320 K (*a*) become almost symmetric at 100 K (*b*)

$[Fe_2(CO)_9]$ in which three symmetric bridging carbonyl ligands span the Fe–Fe bond.[17] This bond is 2.523(1) Å, thus the difference (0.017 Å) between this triply bridged bond and the length of the doubly bridged bond in $[Fe_3(CO)_{12}]$ at the lowest temperature is almost the same as that between 320 and 100 K (0.014 Å), and is even smaller if a comparison is made with the Cotton and Troup [7b] structure (0.018 Å). Hence, a third bridging ligand produces the same effect as bridge symmetrization. The Fe–C length for the bridging ligands in $[Fe_2(CO)_9]$ is also strictly comparable to the values found in the $[Fe_3(CO)_{12}]$ symmetric situation at 100 K [2.016(3) *vs.* 2.00(1) Å (av.)].

The structural information listed in Table 2 can be compared with that collected in Table 3 concerning systems related to $[Fe_3(CO)_{12}]$.[4d,8,19–25] In crystalline $[Fe_2Os(CO)_{12}]$, for instance, there are two independent molecules in the non-centrosymmetric space group *Pn*.[8] The crystal is also affected by disorder of the 'star-of-David' type although the percentage of molecules in the alternative orientation is very small (*ca.* 8%) so that the structural features of the principal images are not affected greatly. The carbonyl ligand distribution in this complex is the same as in $[Fe_3(CO)_{12}]$. The Fe–Fe bond is slightly longer than in $[Fe_3(CO)_{12}]$ [2.589(4) and 2.594(4) Å] and the bridging carbonyls are asymmetric although the degree of asymmetry is different in the two molecules (Table 3). In keeping with our results, Churchill and Fettinger[8] suggested that these differences indicated that 'the energy profile from the asymmetrically bridging case to the symmetrically bridging case is very flat and in the same energetic range as weak intermolecular forces'. A similar situation is observed in the co-crystal formed by the two isomers of $[Fe_3(CO)_{11}(PPh_3)]$. The two molecules differ in the bonding site of the phosphine ligand but possess the same bridging carbonyl ligand distribution as the parent molecule. An analogous bond length distribution is observed in the tris(substituted) derivatives

Table 3 Relevant structural parameters for $[Fe_3(CO)_{12}]$ derivatives

Complex	Fe–Fe (unbridged)	Fe–Fe (bridged)	Fe–C_b(1)	Fe–C_b(2)	Reference
$[Fe_3(CO)_9(PMe_2Ph)_3]$	2.688(7)	2.540(7)	1.97(2)	2.02(3)	19
	2.689(7)		1.97(3)	2.04(3)	
$[Fe_3(CO)_{10}\{P(OMe)_3\}_2]$	2.686(4)	2.533(3)	1.886(22)	2.090(18)	4*d*
	2.683(3)		2.110(1)	1.908(10)	
$[Fe_3(CO)_{10}(\mu\text{-}CNCF_3)\{P(OMe)_3\}]$					20
Isomer 4(II)c	2.679(4)	2.529(4)	1.90(2)	1.96(2)	
	2.709(4)		2.00(2)	1.90(2)	
Isomer 4(I)c	2.685(2)	2.512(2)	1.89(1)	1.97(1)	
	2.682(2)		2.09(1)	1.92(1)	
$[Fe_3(CO)_{10}(\mu\text{-}CNCF_3)(PMe_3)]$	2.672(7)	2.512(7)	1.88(3)	1.91(3)	20
	2.687(7)		2.07(3)	1.89(3)	
$[Fe_3(CO)_{10}(CNBu^t)_2]$	2.702(2)	2.553(1)	1.995(8)	1.986(7)	21
	2.696(1)		1.987(8)	1.975(8)	
$[Fe_3(CO)_{11}(NCC_6H_4Me\text{-}2)]$	2.831(7)	2.551(4)	2.185(27)	1.901(24)	22
	2.788(7)		1.900(27)	1.850(24)	
$[Fe_3(CO)_{10}\{Me_2AsC{=}\overline{CAs(Me)_2CF_2CF_2}\}]$					23
Molecule 1	2.652(8)	2.527(6)	1.91	2.02	
	2.651(7)		1.98	1.90	
Molecule 2	2.643(7)	2.571(7)	2.01	1.95	
	2.671(9)		1.94	2.06	
$[Fe_3(CO)_{11}(CNBu^t)]$	2.687(1)	2.563(1)	2.018(6)	2.018(5)	24
	2.691(1)		2.040(6)	2.008(5)	
$[Fe_3(CO)_{11}(PPh_3)]$					25
Isomer A	2.703(9)	2.568(9)	1.86(4)	1.99(4)	
	2.666(8)		2.04(4)	1.90(4)	
Isomer B	2.703(9)	2.558(9)	1.85(5)	2.07(4)	
	2.711(9)		2.04(5)	1.86(4)	
$[Fe_2Os(CO)_{12}]$					8
Molecule 1		2.589(4)	2.245(16)	1.918(17)	
			1.939(16)	2.224(16)	
Molecule 2		2.594(4)	2.084(20)	1.937(17)	
			2.047(19)	2.123(17)	

$[Fe_3(CO)_9(PMe_2Ph)_3]$ and in several others of the complexes listed in Table 3.

Thermal Motion Analysis.—Thermal motion at the various temperatures has been studied by analysing the anisotropic displacement parameters.[26] Rigid-body motion is described by the *T*, *L* and *S* (translational, librational and screw) tensors, whose values can be derived from the anisotropic displacement parameters.[27] When the molecule is structurally non-rigid, as in the case of $[Fe_3(CO)_{12}]$, the molecular rigid-body motion cannot fully account for the motion of atomic groupings possessing additional motional freedom. It is possible to investigate the non-rigid intramolecular motion of such internally moving groups by defining appropriate librational axes.

Before describing the results, it is relevant to stress that, although at all temperatures a fairly good resolution ($\sin\theta_{max}$ = 0.6) could be achieved by collecting a large number of high-angle diffraction data (see Experimental section), the level of accuracy of the atomic anisotropic displacement parameters for $[Fe_3(CO)_{12}]$ is low. The system is affected by a rather unpleasant disorder, which, amongst other things, causes increase of the thermal diffuse scattering and decreases the intensities of the Bragg reflections. Furthermore, because of the centre of symmetry, the carbon and oxygen atoms of the carbonyl ligands belonging to the two disordered images almost overlap. The electron density around some carbon atoms is smeared out by the thermal motion between atoms at an apparent distance close to resolution. The most reliable displacement parameters are therefore those of the iron atoms (the iron atoms belonging to the centrosymmetric images are *ca.* 1.6 Å apart), and we will focus on the motion of these atoms only. All light atoms will, nonetheless, have to be included in the calculation of the *T*, *L* and *S* tensors in order to avoid the singularity problem associated with the motion of a flat triangular fragment.

A projection of the iron atom displacement parameters for the 320, 160 and 100 K determinations along an axis perpendicular to the metal triangle is shown in Fig. 3. A view along the molecular pseudo-two-fold axis is shown in Fig. 4.

The anisotropic displacement parameters of the iron atoms at the various temperatures are compared in Table 4. It can be seen that the diagonal terms (U_{11}, U_{22} and U_{33}) show a congruent behaviour with the temperature.

(*i*) At all temperatures U_{22} of Fe(2) and Fe(3) is larger than U_{22} of Fe(1). Since the iron triangle is almost perpendicular to the *b* axis, this trend in the U_{22} values indicates that the Fe(2) and Fe(3) displacements, roughly in the *y* direction, are larger than for Fe(1).

(*ii*) U_{22} for the Fe(2) and Fe(3) is larger than U_{11} and U_{33} for the same atoms, while U_{22} is comparable to U_{22} and U_{33} for Fe(1) at all temperatures. This indicates a substantial isotropic displacement from equilibrium for Fe(1), whereas the displacements are largely anisotropic for Fe(2) and Fe(3).

(*iii*) If one considers that the values of the iron atom parameters are derived from the refinement of different data sets, collected at different temperatures, on different diffractometers and on different crystal specimens, the good agreement between all these parameters is remarkable. The iron atom

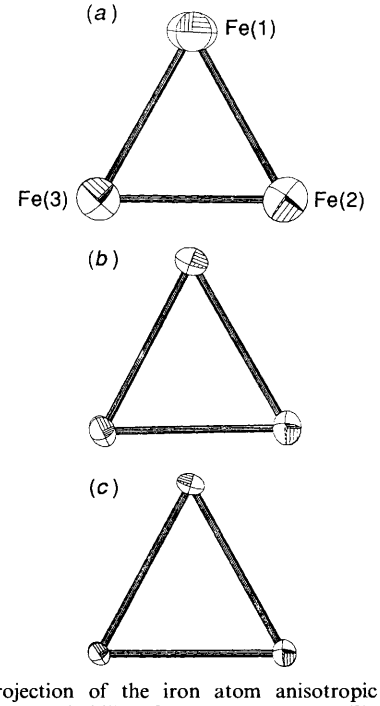

Fig. 3 A projection of the iron atom anisotropic displacement parameters (50% probability) for the 320 (*a*), 160 (*b*) and 100 K (*c*) determinations along an axis perpendicular to the metal triangle

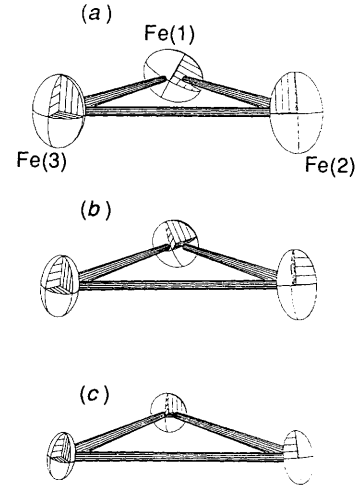

Fig. 4 View along the molecular pseudo-two-fold axis of the iron atom anisotropic displacement parameters (50% probability) for the 320 (*a*), 160 (*b*) and 100 K (*c*) determinations

Table 4 Anisotropic displacement parameters for the iron atoms at various temperatures

	U_{11}	U_{22}	U_{33}	U_{23}	U_{23}	U_{12}
T = 320 K						
Fe(1)	51(1)	49(1)	33(1)	−5(1)	1(1)	5(1)
Fe(2)	43(1)	121(1)	43(1)	−8(1)	1(1)	22(1)
Fe(3)	38(1)	105(1)	45(1)	−25(1)	2(1)	9(1)
T = 295 K (ref. 7*b*)						
Fe(1)	46(2)	43(1)	31(1)	−3(1)	2(1)	4(1)
Fe(2)	37(2)	105(2)	41(1)	−7(1)	1(1)	20(1)
Fe(3)	35(2)	91(2)	40(1)	−21(1)	4(1)	7(1)
T = 250 K						
Fe(1)	46(1)	33(1)	23(1)	−4(1)	2(1)	3(1)
Fe(2)	38(1)	79(1)	29(1)	−6(1)	1(1)	14(1)
Fe(3)	35(1)	66(1)	33(1)	−16(1)	4(1)	4(1)
T = 160 K						
Fe(1)	23(1)	24(1)	17(1)	−4(1)	3(1)	1(1)
Fe(2)	20(1)	50(1)	24(1)	−1(1)	3(1)	12(1)
Fe(3)	15(1)	42(1)	23(1)	−13(1)	4(1)	1(1)
T = 100 K						
Fe(1)	16(1)	18(1)	10(1)	−4(1)	1(1)	1(1)
Fe(2)	14(1)	33(1)	14(1)	−1(1)	2(1)	8(1)
Fe(3)	10(1)	28(1)	13(1)	−9(1)	2(1)	1(1)

parameters obtained by Cotton and Troup[7b] also fit perfectly in the graph.

(*iv*) Such a homogeneous trend strongly indicates that the decrease with temperature of these parameters (at least for the iron atoms) reflects a dynamic behaviour. If the elongation were caused only (or mainly) by some type of static disorder, a 'ferrocene-type' effect would be observed,[12,13] *viz.* the parameters would show no marked temperature dependence.

(*v*) It is true, however, that the persistence, even at 100 K, of the preferential orientation, discussed above in (*i*), could be masking some problem: either the librational motion of the iron triangle is still dominating the motion of the cluster framework or there is a component of static disorder which overlaps the dynamic disorder revealed by the temperature dependence illustrated above. This question could be answered only by collecting data at a much lower temperature.

The analysis of the *L* tensors throws some light on the nature of the dynamic process. Two models of libration of the iron triangle have been explored, namely libration about the pseudo-three-fold axis and libration about the pseudo-two-fold axis passing between Fe(2) and Fe(3). The results are reported in Table 5 and can be summarized as follows. The rigid-body component of the librational motion is almost identical in the two models and decreases on lowering the temperature, although it is little affected between 320 and 250 K. The extra-motion about the three-fold axis is small even at 320 K [0.9 (degree)^2] and is almost neligible below 250 K. The extra motion about the two-fold axis, however, is very large at all temperatures and homogeneously decreases from 130 (degree)^2 at 320 K to 25 (degree)^2 at 100 K. This is in agreement with the preferential elongation of the anisotropic displacement parameters of Fe(2) and Fe(3) in the *y* direction. The same calculations carried out with Cotton and Troup's data[7b] give results that agree perfectly with this picture of the librational motion.

Crystal Structure Decoding.—We have discussed on several other occasions how the structure of a given molecular crystal can be *decoded* by studying the number, distribution and pattern of intermolecular interactions between a reference molecule in the crystal and its first-neighbouring molecules.[15] Our approach is based on the use of atom–atom pairwise potential-energy functions[28] (see Experimental section) to characterize and describe the pattern of intermolecular interactions that are responsible for crystal stability and cohesion. Although the application of this method, originally developed to investigate molecular crystals of organic substances,[29] requires some additional, far from trivial approximations, it has provided valuable insights in a number of crystal chemistry problems. The disorder in crystalline $[Fe_3(CO)_{12}]$, however, severely hinders this type of analysis because the presence of average molecular objects cannot be handled efficaciously by a method that requires an exact knowledge of the interatomic separations.

In order to tackle this problem we have investigated the two limiting ordered molecular distributions which, once averaged, would represent the experimental crystal structure. These are: (*i*) a monoclinic $P2_1$ crystal form obtained from the experimental crystal structure by removing the centre of inversion. The resulting unit cell contains two molecules related only by the screw-axis and (*ii*) a triclinic $P\bar{1}$ crystal form in which one of the two molecules contained in the asymmetric unit ($Z = 2$) is the centrosymmetric one generated from the reference one by the 2_1 axis of the osberved $P2_1/n$ cell. The symmetry relationship between the two molecules in the cell is represented in Fig. 5.

Molecular volumes calculated by the integration method,[30a,b] packing coefficients and atom–atom packing potential energies for the two limiting structures at the various temperatures are compared in Table 6. From this Table it can be appreciated that as the temperature decreases (*i*) the cell volume consistently decreases, as expected; (*ii*) molecular volumes show only a very minor change (the same behaviour is observed if molecular volumes are calculated by the intersecting cups method.[30c] The difference between the values calculated with the more accurate integration method is *ca.* 4 Å^3); (*iii*) the packing coefficient increases, mainly because the cell volume decreases; (*iv*) the packing potential energies for the two limiting crystals become progressively more cohesive; (*v*) in spite of the different molecular distribution in the two crystals and, therefore, of the different sets of intermolecular interactions, the potential energies appear to be comparable at all temperatures for the two crystal models.

Table 5 Libration of the iron triangle around either a three- or two-fold axis

	Rigid-body libration tensor/(degree)^2		IMG additional motion tensor/(degree)^2	
T/K	Two-fold axis	Three-fold axis	Two-fold axis	Three-fold axis
320	12.2(4.0)	12.2(4.0)	130(11)	0.9(2)
295[7b]	13.9(4.0)	13.1(4.0)	109(8.5)	−1(6)
250	12.2(4.0)	9.5(3.0)	80.2(9.1)	1(2)
160	8.8(3.0)	6.3(3.0)	38.9(6.2)	1(2)
100	6.7(3.0)	5.4(2.0)	25.0(4.0)	−1(1)

Table 6 Molecular volumes, packing coefficients and packing potential energies (p.p.e.) for the two limiting $P2_1$ and $P\bar{1}$ structures at various temperatures

				p.p.e./kcal mol^{-1}	
T/K	U_{cell}/Å^3	U_{mol}/Å^3	Packing coefficient	$P2_1$	$P\bar{1}$
320	836.52	281.03	0.67	−50.51	−51.05
295	831.50	280.97	0.68	−51.09	−50.70
250	816.82	280.35	0.69	−51.87	−52.28
160	795.44	280.90	0.71	−52.65	−52.62
100	784.92	280.50	0.72	−53.84	−53.54

The description of the crystal structure of $[Fe_3(CO)_{12}]$ in the two limiting systems allows us to explore in detail also the pattern of closest neighbouring atom–atom interactions. The basic assumption is that all 'true' intermolecular interactions are necessarily represented by either set. Table 7 reports a comparison of the distance and energies for the shortest intermolecular contacts in the limiting $P2_1$ and pseudo-$P\bar{1}$ crystals and their variation with temperature.

The intermolecular contact distances listed in Table 7 show, in general, the expected shortening as the temperature decreases. This is accompanied by an increase in the repulsive terms of the atom–atom interactions as the atoms are brought closer together.

The interaction C(9)···O(11) is present in both model crystals because it joins molecules related by translational symmetry as shown in Fig. 6. This interaction decreases by 0.206 Å on going from 320 to 100 K (the corresponding energy increases from 0.016 to 0.305 kcal mol^{-1}). It is interesting to postulate that this change causes an intramolecular 'pressure' on the bridging ligand CO(2) which is thus pushed towards a more symmetric position to alleviate the intermolecular repulsions along the *a* axis. The intramolecular separation between O(9) and O(11) accordingly decreases from 5.982 Å in Cotton and Troup's structure[7b] to 5.923 Å at 100 K. The other bridging ligand is less affected by the intramolecular surroundings, the symmetrization in this case is seemingly needed in order to maintain homogeneous electronic distribution on the two metal atoms carrying the bridging ligands. Table 7 also shows the variation with temperature of the intermolecular O(1)···O(2) contact distance which extends roughly along the *b* axis. Although this interaction does not give

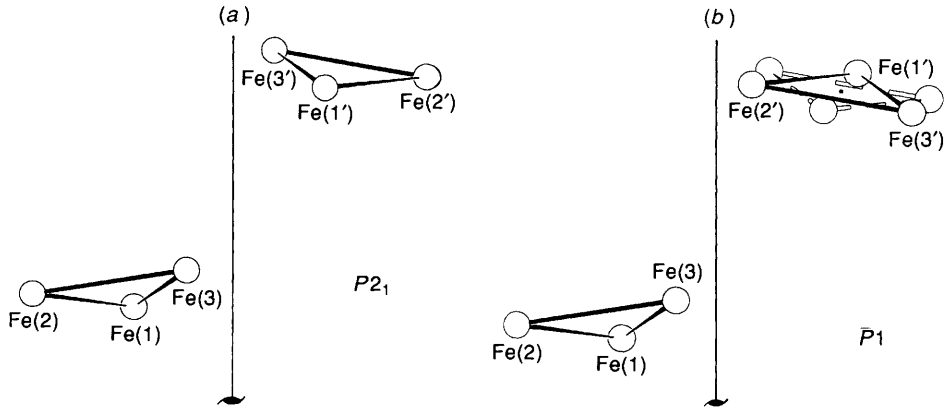

Fig. 5 Schematic representation of the relationship between the two molecules forming the limiting $P2_1$ (*a*) and pseudo-$P\bar{1}$ crystals (*b*)

Table 7 Comparison of the distance (d/Å) and atom–atom interaction energies (E/kcal mol^{-1}) for the shortest intermolecular contacts and their variation with temperature in the limiting $P2_1$ and pseudo-$P\bar{1}$ crystals

	T/K				
Contact	320 d/Å (E/kcal mol^{-1})	295 d/Å (E/kcal mol^{-1})	250 d/Å (E/kcal mol^{-1})	160 d/Å (E/kcal mol^{-1})	100 d/Å (E/kcal mol^{-1})
$P2_1$ crystal					
C(9)···O(11)	3.117 (0.016)	3.059 (0.069)	3.048 (0.082)	2.930 (0.264)	2.911 (0.305)
O(1)···O(2)	3.368 (–)	3.264 (–)	3.116 (–)	3.105 (–)	3.087 (–)
O(3)···O(5)	3.126 (–)	2.989 (–0.072)	2.791 (0.117)	2.965 (–0.060)	2.916 (–0.027)
O(4)···O(5)	3.074 (–0.103)	3.012 (–0.083)	3.130 (–)	2.757 (0.178)	2.754 (0.183)
pseudo-$P\bar{1}$ crystal					
C(9)···O(11)	3.117 (0.016)	3.059 (0.069)	3.048 (0.082)	2.930 (0.264)	2.911 (0.305)
O(1)···O(2)	3.368 (–)	3.264 (–)	3.116 (–)	3.105 (–)	3.087 (–)
O(3)···C(7)	3.222 (–0.047)	3.066 (0.062)	3.011 (0.128)	2.943 (0.240)	2.932 (0.260)
O(4)···O(7)	2.978 (–0.067)	3.012 (–0.083)	2.856 (0.030)	3.023 (–0.087)	2.964 (–0.059)

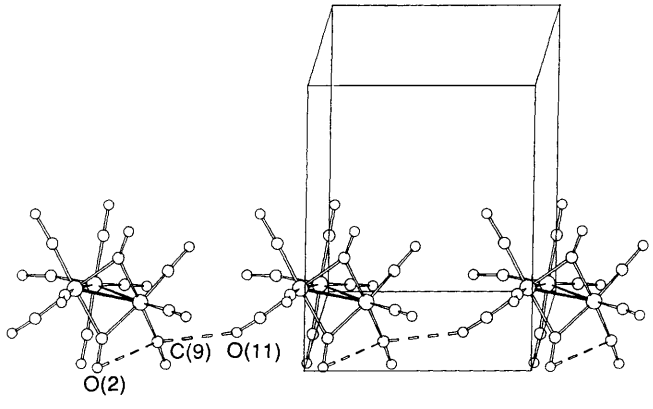

Fig. 6 The row of molecules extending in the x direction. Note how the carbonyls CO(9) and CO(11) interact *via* C(9)···O(11) contacts

rise to atom–atom repulsions (within the limits of the potential parameters herein adopted), it is noteworthy that it shows the largest variation between the limiting temperatures (Δ = 0.28 Å). This is indicative of the extent of interpenetration of the molecules as the temperature is decreased. It should also be taken into account that this close approach accompanies the symmetrization of the bridging ligands. Were it not for this change, these intermolecular interactions would probably 'oppose' the temperature decrease and, perhaps, lead to a change in crystal structure through a phase transition. Since the difference in energy between asymmetric and symmetric bridging is very small, the symmetrization of the bridging systems is preferred to an increase of intermolecular repulsions between next neighbouring molecules. In other words, in the case of $[Fe_3(CO)_{12}]$ it is less expensive to change the molecular, than the crystal, structure.

Conclusion

In this paper we have discussed our results of the variable-temperature investigation of the molecular and crystal structure of $[Fe_3(CO)_{12}]$. Our observations can be summarized as follows. (*i*) At higher temperatures the asymmetric structure is favoured. This appears to be an 'intrinsic' structural feature of $[Fe_3(CO)_{12}]$ and of its derivatives. Most complexes obtained by substitution of one or more carbonyl ligands maintain the asymmetric bridging pattern. Since this is observed in several complexes irrespective of the type, number and site of bonding of the substituents and within different crystal structures the deviation from C_{2v} symmetry appears to have primarily an

intramolecular origin. (*ii*) On decreasing the temperature the bridges become more symmetric and the bridged Fe–Fe bond shortens. The 'symmetrization' of the bridging carbonyls and the decrease in Fe–Fe separation along the bridged bond is homogeneous and significant in the temperature range explored. (*iii*) The displacement parameters of the bridged iron atoms are markedly anisotropic; showing at all temperatures a preferential elongation perpendicular to the plane defined by the iron atoms. In the 'dynamic' interpretation of this disorder, this indicates that the oscillatory motion of the iron triangle about the molecular two-fold axis is operating at all temperatures. As the temperature decreases the displacement is reduced but not cancelled. (*iv*) The lowest-energy structure, in fact, is not frozen out even at 100 K as indicated by the persistence of an anisotropic orientation of the bridged iron atom and by a slight asymmetry of the carbonyl bridges. The presence of a component of static disorder cannot be completely ruled out by our experiments. Only at very low temperature could the oscillatory motion of the two iron atoms, in principle, be stopped completely. It is worth recalling here that the displacement parameters of the iron atoms in the isostructural species $[Fe_2Os(CO)_{12}]$ show a similar preferential orientation.

It would appear that the temperature decrease has a two-fold effect on the crowded structure of $[Fe_3(CO)_{12}]$: (*i*) the decrease in atomic motion allows the atoms *within the same molecule* to get closer together and (*ii*) the decrease in molecular motion increases the interpenetration of the molecules *within the crystal* and an increase of the 'steric pressure' of the surroundings. The molecular structure is, therefore, 'driven' towards the bonding situation corresponding to C_{2v} symmetry with symmetric bridging carbonyl ligands and, consequently, with shorter Fe–Fe bond length. This is in qualitative agreement with the temperature dependence shown by the Mössbauer spectrum of $[Fe_3(CO)_{12}]$.[5b] As mentioned in the Introduction, this behaviour had been related to changes in orbital population resulting from changes in interatomic bond distances. It would appear that the asymmetry of the bridging carbonyls alleviates destabilizing steric intramolecular interactions which are more relevant at higher than at lower temperatures because the carbonyl ligands undergoing thermal oscillations 'require more space' and clash with each other. This is in keeping with a number of concurring pieces of evidence in support of the idea that transition-metal cluster molecules are plastic systems formed by ligands packed about soft metallic cores.[31]

Experimental

Diffraction Experiments.—Diffraction intensities were all measured on an Enraf–Nonius CAD-4 diffractometer. This was equipped with an Enraf–Nonius low-temperature device operating with liquid nitrogen for the data sets at 320, 250 and 160 K[7c] collected at the University of Bologna. The data set at 100 K was collected at the University of Glasgow using an Oxford Cryosystems Cryostream cooler. Different crystal specimens were used for all data collections. Diffraction data were corrected for absorption by azimuthal scanning of high-χ reflections. All atoms were allowed to vibrate anisotropically. The programs SHELX 86[32a] and SHELXL 93[32b] were used for data treatment and refinement based on F^2. Crystal data and details of measurements are reported in Table 8 and fractional atomic coordinates, obtained from the 100 K data set, in Table 9.

Additional material available from the Cambridge Crystallographic Data Centre comprises thermal parameters and remaining bond lengths and angles.

Crystal Packing Decoding.—The efficiency of volume occupation in the crystal can be evaluated by estimating the packing coefficients (p.c.) from the relationship p.c. = $U_{mol}Z/U_{cell}$ where U_{mol} represents the van der Waals molecular volume (van der Waals radii of 2.15, 1.75 and 1.50 Å for Fe, C and O respectively). These volumes have been estimated with the integration method put forward by Gavezzotti[30a,b] and compared with the values obtained with the slightly cruder 'intersecting cups' model of Kitaigorodsky.[30c] The volumes calculated with the integration steps method are usually larger than those calculated with this latter method.

The packing potential energy (p.p.e.) of an organometallic molecule can be estimated by applying empirical methods similar to those usually employed in the neighbouring field of solid-state organic chemistry. Use is made of the expression p.p.e. = $\Sigma_i\Sigma_j[A\exp(-Br_{ij}) - Cr_{ij}^{-6}]$, where r_{ij} represents the non-bonded atom–atom intermolecular distance and the

Table 8 Crystal data and details of measurements

	T/K			
	320	250	160	100
Crystal dimensions/mm	0.15 × 0.18 × 0.14	0.15 × 0.18 × 0.14	0.15 × 0.18 × 0.14	0.16 × 0.20 × 0.15
a/Å	8.375(2)	8.304(2)	8.221(4)	8.174(2)
b/Å	11.330(2)	11.231(4)	11.128(3)	11.090(2)
c/Å	8.882(4)	8.822(3)	8.760(4)	8.722(3)
β/°	97.00(3)	96.89(4)	96.99(3)	96.90(2)
U/Å^3	836.5(4)	816.8(4)	795.4(6)	784.9(4)
μ(Mo-Kα)/cm^{-1}	26.29	26.93	27.65	28.02
θ range/°	3–30	3–30	3–35	3–40
ω scan width/°	0.70	0.80	0.70	
Octants explored (*hkl*)	−11 to +11	−11 to +11	−13 to +13	−14 to +11
	0–15	0–15	0–17	0–20
	0–12	0–12	0–10	0–15
Measured reflections	2564	2500	3020	4083
Unique observed reflections	2427	2366	2730	3941
Unique observed reflections [$I_o > 2\sigma(I_o)$]	1160	1007	1521	2648
Goodness of fit on F^2	1.086	1.028	1.196	1.034
Final $R(F)$ [$I > 2\sigma(I)$]	0.046	0.068	0.058	0.070
R' (on all data)	0.132	0.164	0.142	0.124
Final $R(F^2)$ [$I > 2\sigma(I)$]	0.135	0.183	0.130	0.177
wR_2 (all data)	0.175	0.232	0.172	0.211

Details in common: M = 503.67, monoclinic, space group $P2_1/n$, Z = 2, $F(000)$ = 492, λ(Mo-Kα) = 0.710 69 Å, number of refined parameters = 244; $R(F) = \Sigma|F_o - F_c|/\Sigma(F_o)$; $R' = \Sigma w|F_o - F_c|/\Sigma wF_o$; $R(F^2) = \Sigma(F_o^2 - F_c^2)/\Sigma F_o^2$; $wR_2 = [\Sigma w(F_o^2 - F_c^2)^2/\Sigma w(F_o^2)^2]^{\frac{1}{2}}$.

Table 9 Fractional atomic coordinates for $[Fe_3(CO)_{12}]$ at 100 K

Atom	*x*	*y*	*z*
Fe(1)	−555(1)	−210(1)	−1685(1)
Fe(2)	1783(1)	−150(1)	739(1)
Fe(3)	−1135(1)	428(1)	1167(1)
C(1)	797(27)	1455(10)	1145(20)
O(1)	1277(11)	2428(7)	1363(9)
C(2)	207(22)	−1077(11)	1881(21)
O(2)	88(11)	−1955(7)	2537(8)
C(3)	−822(26)	−1770(9)	−1188(20)
O(3)	−1035(11)	−2771(6)	−942(10)
C(4)	−210(26)	1419(11)	−1995(21)
O(4)	7(10)	2380(6)	−2306(9)
C(5)	−2606(10)	−191(7)	−2707(8)
O(5)	−3924(35)	−328(24)	−3323(33)
C(6)	638(10)	−625(6)	−3219(8)
O(6)	1540(34)	−1001(19)	−4149(20)
C(7)	3242(11)	62(8)	2436(10)
O(7)	4165(34)	121(22)	3468(31)
C(8)	2896(23)	585(20)	−583(26)
O(8)	3731(12)	1181(11)	−1335(9)
C(9)	2499(9)	−1653(8)	236(10)
O(9)	2867(25)	−2598(14)	−116(20)
C(10)	−1370(9)	761(6)	3141(7)
O(10)	−1409(33)	808(17)	4406(18)
C(11)	−2908(26)	−663(18)	870(25)
O(11)	−3964(13)	−1223(11)	737(11)
C(12)	−2243(9)	1768(9)	393(10)
O(12)	−3026(30)	2627(20)	−172(21)

indexes *i* and *j* in the summation run over all atoms of the reference molecule and over the atoms of the surrounding molecules within a pre-set cut-off distance (usually 15 Å with large cluster systems), respectively. The iron atoms were attributed the potential coefficients available for krypton. The calculation procedures of U_{mol}, p.c. and p.p.e. are all implemented within Gavezzotti's OPEC suite of programs.[30a] SCHAKAL 93[33] was used for the graphical representation of the results.

Acknowledgements

D. B. and F. G. thank the Ministero dell'Università e della Ricerca Scientifica e Tecnologica (Italy) and L. J. F. the SERC for financial support and D. B., F. G. and B. F. G. J. acknowledge NATO for a travel grant.

References

1 (*a*) M. Poliakoff and J. J. Turner, *Chem. Commun.*, 1970, 1008; (*b*) J. Knight and M. J. Mays, *Chem. Commun.*, 1970, 1006; (*c*) F. A. Cotton and D. L. Hunter, *Inorg. Chim. Acta*, 1974, **11**, L9; (*d*) G. R. Dobson and R. K. Sheline, *Inorg. Chem.*, 1963, **2**, 1313.

2 S. Aime, M. Botta, R. Gobetto and D. Osella, *J. Chem. Soc., Dalton Trans.*, 1988, 791; S. Aime, M. Botta, O. Gambino, R. Gobetto and D. Osella, *J. Chem. Soc., Dalton Trans.*, 1989, 1277; A. Foster, B. F. G. Johnson, J. Lewis, T. W. Matheson, B. H. Robinson and W. G. Jackson, *J. Chem. Soc., Chem. Commun.*, 1974, 1042; R. E. Benfield, P. D. Gavens, B. F. G. Johnson, M. J. Mays, S. Aime, L. Milone and D. Osella, *J. Chem. Soc., Dalton Trans.*, 1981, 1535; D. H. Farrar and J. A. Lunniss, *J. Chem. Soc., Dalton Trans.*, 1987, 1249.

3 (*a*) B. F. G. Johnson and R. E. Benfield, *Transition Metal Clusters*, ed. B. F. G. Johnson, Wiley, New York, 1980, p. 471 and refs. therein; (*b*) B. F. G. Johnson, E. Parisini and Y. V. Roberts, *Organometallics*, 1993, **12**, 233; (*c*) B. F. G. Johnson, E. Parisini and Y. V. Roberts, *J. Chem. Soc., Dalton Trans.*, 1992, 2573; (*d*) B. F. Mann, *Organometallics*, 1993, **12**, 233.

4 (*a*) H. Dorn, B. E. Hanson and E. Motell, *Inorg. Chim. Acta*, 1981, **54**, L71; (*b*) B. E. Hanson, E. C. Lisic, J. T. Petty and G. A. Iannacone, *Inorg. Chem.*, 1986, **25**, 4062; (*c*) T. H. Walter, L. Reven and E. Oldfield, *J. Phys. Chem.*, 1989, **93**, 1320; (*d*) H. Adams, N. A. Bailey, G. W. Bentley and B. E. Mann, *J. Chem. Soc., Dalton Trans.*, 1989, 1831.

5 (*a*) N. E. Erickson and A. W. Fairhall, *Inorg. Chem.*, 1965, **4**, 1320; (*b*) C. G. Benson, G. J. Long, J. W. Kolis and D. F. Shivers, *J. Am. Chem. Soc.*, 1985, **107**, 5297.

6 B. Binsted, J. Evans, G. N. Greaves and R. J. Prince, *J. Chem. Soc., Chem. Commun.*, 1987, 1330.

7 (*a*) C. H. Wei and L. F. Dahl, *J. Am. Chem. Soc.*, 1969, **91**, 1351; (*b*) F. A. Cotton and J. M. Troup, *J. Am. Chem. Soc.*, 1974, **96**, 4155; (*c*) D. Braga, F. Grepioni, L. J. Farrugia and B. F. G. Johnson, *J. Organomet. Chem.*, 1994, **464**, C39.

8 M. R. Churchill and J. C. Fettinger, *Organometallics*, 1990, **9**, 752.

9 D. Braga and F. Grepioni, *Organometallics*, 1991, **10**, 1254.

10 D. Braga, A. W. Bott, C. E. Anson, B. F. G. Johnson and E. A. Marseglia, *J. Chem. Soc., Dalton Trans.*, 1990, 3517.

11 (*a*) J. W. Lauher, *J. Am. Chem. Soc.*, 1986, **108**, 1521; (*b*) J. Li and K. Jug, *Inorg. Chim. Acta*, 1992, **196**, 89; (*c*) D. Braga, A. Rodger and B. F. G. Johnson, *Inorg. Chim. Acta*, 1990, **174**, 185.

12 F. Takusagawa and T. F. Koetzle, *Acta Crystallogr., Sect. B*, 1979, **35**, 1074.

13 P. Seiler and J. D. Dunitz, *Acta Crystallogr., Sect. B*, 1979, **35**, 1068, 2020.

14 D. Braga, F. Grepioni, P. Sabatino and A. Gavezzotti, *J. Chem. Soc., Dalton Trans.*, 1992, 1185.

15 D. Braga and F. Grepioni, *Acc. Chem. Res.*, 1994, **27**, 51.

16 R. Desirato, jun., and G. R. Dobson, *J. Chem. Educ.*, 1982, **59**, 752.

17 C. K. Johnson, ORTEP, Report ORNL-5138, Oak Ridge National Laboratory, Oak Ridge, TN, 1976.

18 F. A. Cotton and J. M. Troup, *J. Chem. Soc., Dalton Trans.*, 1974, 800.

19 G. Raper and W. S. McDonald, *J. Chem. Soc. A*, 1971, 3430.

20 D. Lentz and R. Marschall, *Organometallics*, 1991, **10**, 1487.

21 J. B. Murray, B. K. Nicholson and A. Whitton, *J. Organomet. Chem.*, 1990, **385**, 91.

22 C. J. Cardin, D. J. Cardin, N. B. Kelly, G. A. Lawless and M. B. Power, *J. Organomet. Chem.*, 1988, **341**, 447.

23 P. J. Roberts, B. R. Penfold and J. Trotter, *Inorg. Chem.*, 1970, **9**, 2137.

24 M. I. Bruce, T. W. Hambley and B. K. Nicholson, *J. Chem. Soc., Dalton Trans.*, 1983, 2385.

25 D. J. Dahm and R. A. Jacobson, *J. Am. Chem. Soc.*, 1968, **90**, 5106.

26 J. D. Dunitz, V. Schomaker and K. N. Trueblood, *J. Phys. Chem.*, 1988, **82**, 856.

27 K. N. Trueblood, THMA11, Thermal Motion Analysis Computer Program, University of California, Los Angeles, 1990.

28 A. J. Pertsin and A. I. Kitaigorodsky, *The Atom–Atom Potential Method*, Springer, Berlin, 1987.

29 A. Gavezzotti and M. Simonetta, *Chem. Rev.*, 1981, **82**, 1; Z. Berkovitch-Yellin and L. Leiserowitz, *J. Am. Chem. Soc.*, 1982, **104**, 4052; G. R. Desiraju, *Crystal Engineering, The Design of Organic Solids*, Elsevier, Amsterdam, 1989, p. 47.

30 (*a*) A. Gavezzotti, OPEC, Organic Packing Potential Energy Calculations, University of Milano, 1983; (*b*) A. Gavezzotti, *J. Am. Chem. Soc.*, 1983, **195**, 5220; (*c*) A. I. Kitaigorodsky, Molecular Crystals and Molecules, Academic Press, New York, 1973.

31 V. G. Albano and D. Braga, in *Accurate Molecular Structures*, eds. A. Domenicano and I. Hargittai, Oxford University Press, 1992.

32 G. M. Sheldrick, (*a*) *Acta Crystallogr., Sect. A*, 1990, **46**, 467; (*b*) SHELXL 93, University of Göttingen, 1993.

33 E. Keller, SCHAKAL 93, Graphical Representation of Molecular Models, University of Freiburg, Germany, 1993.

Received 6th April 1994; *Paper* 4/020491